The influence of ozone precursor emissions from four world regions on tropospheric composition and radiative climate forcing

Meridith M. Fry,[1] Vaishali Naik,[2] J. Jason West,[1] M. Daniel Schwarzkopf,[3] Arlene M. Fiore,[3,4] William J. Collins,[5] Frank J. Dentener,[6] Drew T. Shindell,[7] Cyndi Atherton,[8,9] Daniel Bergmann,[8] Bryan N. Duncan,[10] Peter Hess,[11] Ian A. MacKenzie,[12] Elina Marmer,[6,13] Martin G. Schultz,[14] Sophie Szopa,[15] Oliver Wild,[16] and Guang Zeng[17]

Received 8 November 2011; revised 23 February 2012; accepted 4 March 2012; published 13 April 2012.

[1] Ozone (O_3) precursor emissions influence regional and global climate and air quality through changes in tropospheric O_3 and oxidants, which also influence methane (CH_4) and sulfate aerosols (SO_4^{2-}). We examine changes in the tropospheric composition of O_3, CH_4, SO_4^{2-} and global net radiative forcing (RF) for 20% reductions in global CH_4 burden and in anthropogenic O_3 precursor emissions (NO_x, NMVOC, and CO) from four regions (East Asia, Europe and Northern Africa, North America, and South Asia) using the Task Force on Hemispheric Transport of Air Pollution Source-Receptor global chemical transport model (CTM) simulations, assessing uncertainty (mean ± 1 standard deviation) across multiple CTMs. We evaluate steady state O_3 responses, including long-term feedbacks via CH_4. With a radiative transfer model that includes greenhouse gases and the aerosol direct effect, we find that regional NO_x reductions produce global, annually averaged positive net RFs (0.2 ± 0.6 to 1.7 ± 2 mWm^{-2}/Tg N yr^{-1}), with some variation among models. Negative net RFs result from reductions in global CH_4 (−162.6 ± 2 mWm^{-2} for a change from 1760 to 1408 ppbv CH_4) and regional NMVOC (−0.4 ± 0.2 to −0.7 ± 0.2 mWm^{-2}/Tg C yr^{-1}) and CO emissions (−0.13 ± 0.02 to −0.15 ± 0.02 mWm^{-2}/Tg CO yr^{-1}). Including the effect of O_3 on CO_2 uptake by vegetation likely makes these net RFs more negative by −1.9 to −5.2 mWm^{-2}/Tg N yr^{-1}, −0.2 to −0.7 mWm^{-2}/Tg C yr^{-1}, and −0.02 to −0.05 mWm^{-2}/Tg CO yr^{-1}. Net RF impacts reflect the distribution of concentration changes, where RF is affected locally by changes in SO_4^{2-}, regionally to hemispherically by O_3, and globally by CH_4. Global annual average SO_4^{2-} responses to oxidant changes range from 0.4 ± 2.6 to −1.9 ± 1.3 Gg for NO_x reductions, 0.1 ± 1.2 to −0.9 ± 0.8 Gg for NMVOC reductions, and −0.09 ± 0.5 to −0.9 ± 0.8 Gg for CO reductions, suggesting additional research is needed. The 100-year global warming potentials (GWP_{100}) are calculated for the global CH_4 reduction (20.9 ± 3.7 without stratospheric O_3 or water vapor, 24.2 ± 4.2 including those components), and for the regional NO_x, NMVOC, and CO reductions (−18.7 ± 25.9 to −1.9 ± 8.7 for NO_x, 4.8 ± 1.7 to 8.3 ± 1.9 for NMVOC, and 1.5 ± 0.4 to 1.7 ± 0.5 for CO). Variation in GWP_{100} for NO_x, NMVOC, and CO suggests that regionally specific GWPs may be necessary and could support the inclusion

[1]Department of Environmental Sciences and Engineering, University of North Carolina at Chapel Hill, Chapel Hill, North Carolina, USA.
[2]Atmospheric Physics, Chemistry, and Climate Group, UCAR GFDL, Princeton, New Jersey, USA.
[3]Atmospheric Physics, Chemistry, and Climate Group, NOAA GFDL, Princeton, New Jersey, USA.
[4]Now at Lamont-Doherty Earth Observatory, Palisades, New York, USA.
[5]Met Office Hadley Centre, Exeter, UK.
[6]Institute for Environment and Sustainability, DG-Joint Research Centre, European Commission, Ispra, Italy.
[7]NASA Goddard Institute for Space Studies, New York, New York, USA.
[8]Atmospheric Earth and Energy Division, Lawrence Livermore National Laboratory, Livermore, California, USA.
[9]Now at Gordon and Betty Moore Foundation, Palo Alto, California, USA.
[10]NASA Goddard Space Flight Center, Greenbelt, Maryland, USA.
[11]Biological and Environmental Engineering, Cornell University, Ithaca, New York, USA.
[12]School of GeoSciences, University of Edinburgh, Edinburgh, UK.
[13]Now at Department of Geography, University of Hamburg, Hamburg, Germany.
[14]Institut für Energie- und Klimaforschung (IEK-8), Forschungszentrum Jülich GmbH, Jülich, Germany.
[15]Laboratoire des Sciences du Climat et de l'Environnement, CEA, IPSL, UVSQ, CNRS, Gif-sur-Yvette, France.
[16]Lancaster Environment Centre, Lancaster University, Lancaster, UK.
[17]National Institute of Water and Atmospheric Research, Lauder, New Zealand.

0148-0227/12/2011JD017134

of O_3 precursors in future policies that address air quality and climate change simultaneously. Both global net RF and GWP_{100} are more sensitive to NO_x and NMVOC reductions from South Asia than the other three regions.

Citation: Fry, M. M., et al. (2012), The influence of ozone precursor emissions from four world regions on tropospheric composition and radiative climate forcing, *J. Geophys. Res.*, *117*, D07306, doi:10.1029/2011JD017134.

1. Introduction

[2] Tropospheric ozone (O_3), methane (CH_4), and aerosols make important contributions to the global mean radiative forcing (RF) of climate [*Forster et al.*, 2007; *Ramaswamy et al.*, 2001]. Here we aim to quantify the net RF of these species due to regional changes in O_3 precursor emissions, across an ensemble of global chemical transport models (CTMs). We define net RF as the net (incoming minus outgoing) change in irradiance (solar and infrared) at the tropopause between a base and perturbed state (in Watts per square meter [W m^{-2}]) after allowing stratospheric temperatures to readjust [*Forster et al.*, 2007]. The contribution of changes in tropospheric O_3 to the global mean RF since preindustrial times is an estimated 0.35 ± 0.15 Wm^{-2}, which is approximately 21% of the RF due to changes in carbon dioxide (CO_2) [*Forster et al.*, 2007]. Changes in CH_4 have contributed approximately 0.48 Wm^{-2}, while those in sulfate aerosols (SO_4^{2-}) have contributed approximately -0.4 ± 0.2 Wm^{-2} (direct effect only) [*Forster et al.*, 2007].

[3] Changes in O_3 precursor emissions (nitrogen oxides [NO_x], non-methane volatile organic compounds [NMVOC], carbon monoxide [CO], and CH_4) affect the abundance of gaseous species (O_3 and CH_4), and aerosols via changes in the availability of atmospheric oxidants (hydroxyl radical [OH], hydrogen peroxide [H_2O_2], O_3) [*Pham et al.*, 1995; *Unger et al.*, 2006; *Shindell et al.*, 2009; *Leibensperger et al.*, 2011]. These perturbations in turn influence the RF due to O_3 and CH_4 and inorganic aerosol-phase species [*Ming et al.*, 2005; *Unger et al.*, 2006; *Naik et al.*, 2007; *Shindell et al.*, 2009]. O_3 precursors also affect organic aerosols, including the formation of secondary organic aerosols (SOA) [*Carlton et al.*, 2010], but the resulting RF remains to be quantified. O_3 decreases plant growth and hence reduces the removal of CO_2 from the atmosphere [*Felzer et al.*, 2007; *Sitch et al.*, 2007; *Collins et al.*, 2010], while NO_x emissions influence nitrogen deposition and the subsequent uptake of CO_2 in terrestrial and oceanic ecosystems [*Holland and Lamarque*, 1997; *Duce et al.*, 2008]. Because of these influences, actions to control O_3 precursor emissions affect both air quality and global climate [*Fiore et al.*, 2002; *Dentener et al.*, 2005; *West et al.*, 2007].

[4] Past studies have shown that both regional and global reductions in NO_x surface emissions produce an overall positive RF from global CH_4 increases via decreases in OH, which outweigh the negative forcing from tropospheric O_3 decreases. The magnitude of forcing, however, depends on the location or sector of emission reduction [*Fuglestvedt et al.*, 1999; *Wild et al.*, 2001; *Berntsen et al.*, 2005; *Naik et al.*, 2005; *West et al.*, 2007; *Derwent et al.*, 2008]. In contrast, CO, NMVOC, and CH_4 reductions contribute an overall negative RF by decreasing tropospheric O_3 and increasing OH, leading to global CH_4 decreases [*Prather*, 1996; *Wild et al.*, 2001; *Fiore et al.*, 2002; *Naik et al.*, 2005]. Global anthropogenic CH_4 emission reductions were shown to produce the most negative RF of the O_3 precursors, mainly due to direct reductions in CH_4 forcing [*Fiore et al.*, 2002; *Shindell et al.*, 2005; *West et al.*, 2007].

[5] Because of the short atmospheric lifetimes of O_3, aerosols, and their precursors (apart from CH_4), studies of regional O_3 precursor reductions show that air quality and RF effects depend strongly on the geographical location of emissions [*Fuglestvedt et al.*, 1999; *Berntsen et al.*, 2005; *Naik et al.*, 2005]. The dependence on location, however, has made it difficult to include O_3 precursors in emissions trading schemes or international climate agreements [*Rypdal et al.*, 2005], and to evaluate the co-benefits of actions to reduce O_3 for slowing global climate change. Studies have shown substantial dependence of O_3 concentrations and RF on the region of NO_x emissions [*Fuglestvedt et al.*, 1999; *Berntsen et al.*, 2005; *Naik et al.*, 2005; *Derwent et al.*, 2008; *Fuglestvedt et al.*, 2010], where O_3 and RF are more sensitive to NO_x reductions from tropical regions, yet positive global annual average net RFs result from NO_x reductions in each of nine world regions [*Naik et al.*, 2005]. While NMVOCs typically have atmospheric lifetimes comparable to NO_x, CO has a longer atmospheric lifetime of 1–3 months [*Seinfeld and Pandis*, 2006], suggesting that the influence of CO on O_3 and OH may be less dependent on reduction region [*Berntsen et al.*, 2005; *Rypdal et al.*, 2005]. Apart from *Naik et al.* [2005], who also examined combined reductions in NO_x, CO, and NMVOCs from three regions, and *Berntsen et al.* [2005], who evaluated CO changes from two regions, less attention has been placed on regional CO and NMVOC emissions and their effects on tropospheric O_3, CH_4, and SO_4^{2-} and global and regional net RF. In response to nonuniform forcings, some regional climate responses are also sensitive to the location and distribution of O_3, aerosols, and RF [*Shindell and Faluvegi*, 2009].

[6] Here we investigate the effects of a 20% reduction in global CH_4 abundance and 20% reductions in anthropogenic emissions of NO_x, NMVOC, and CO, individually and combined, from four world regions on tropospheric O_3, CH_4, and SO_4^{2-} concentrations and on the resulting distribution and magnitude of global net RF for all precursor-region pairs. We use results from an ensemble of global CTMs that participated in the Task Force on Hemispheric Transport of Air Pollution (TF HTAP) multimodel intercomparison study of Source-Receptor (SR) sensitivity [*Fiore et al.*, 2009], which allows for an assessment of uncertainty as the spread across CTMs. We examine the regional dependency of RF and global warming potential (GWP) to individual precursors by comparing estimates across the four regions of reduction.

2. Methodology

[7] We use the results from an ensemble of 11 global CTMs [*Task Force on Hemispheric Transport of Air*

Table 1. HTAP Source-Receptor Sensitivity Simulations, Where the Four Regions of Reduction are East Asia, Europe, North America, and South Asia for SR3 Through SR6

Scenario	Description
SR1	Base simulation
SR2	20% reduction in global CH_4 mixing ratio
SR3	20% reduction in regional NO_x emissions
SR4	20% reduction in regional NMVOC emissions
SR5	20% reduction in regional CO emissions
SR6	20% reduction in regional NO_x, NMVOC, CO, and aerosol emissions

Pollution, 2010] to evaluate changes in the tropospheric distributions of O_3, CH_4, and SO_4^{2-} for each reduction scenario. The net RF is calculated from the simulated changes in O_3, CH_4, and SO_4^{2-} using the standalone radiative transfer model (RTM) developed by the National Oceanographic and Atmospheric Administration (NOAA) Geophysical Fluid Dynamics Laboratory (GFDL) [*Schwarzkopf and Ramaswamy*, 1999; *GFDL Global Atmospheric Model Development Team* (*GFDL GAMDT*), 2004]. We estimate the RF due to SO_4^{2-}, as SO_4^{2-} responds to oxidant changes, considering only its direct effects on radiation [*Naik et al.*, 2007]; few CTMs reported other aerosol species for all reduction scenarios. Although we account for variability across the CTM ensemble in the O_3, SO_4^{2-}, and CH_4 estimates, we likely underestimate the uncertainty in net RF by using only a single RTM.

2.1. HTAP CTM Simulations

[8] The SR simulations performed by each CTM are outlined in Table 1. We analyze O_3 and CH_4 results from 11 CTMs and SO_4^{2-} results from four CTMs (Table 2). Each CTM utilized its own emissions inventory and prescribed meteorological fields for the year 2001 [*Fiore et al.*, 2009]. Anthropogenic emissions of NO_x, NMVOCs, CO, and all precursors combined were reduced by 20% in each of four world regions: East Asia (EA), Europe and Northern Africa (EU), North America (NA), and South Asia (SA). For CH_4, the present-day abundance (1760 parts per billion by volume [ppbv]) was imposed in all simulations except for the CH_4 control simulation (SR2), where global CH_4 abundance was decreased by 20% to 1408 ppbv. All simulations were performed for a full year (2001), after an initial spin-up of at least six months [*Fiore et al.*, 2009].

[9] The multimodel mean ± 1 standard deviation changes in the anthropogenic emissions of NO_x, NMVOCs, and CO, across 11 CTMs, are presented in Table 3. There is considerable variability in the emission reduction magnitudes across CTMs. Coefficients of variation (CVs) (standard deviation/mean) are lowest for NO_x emissions from EU, NA, and SA, while there is more variability in NMVOC and CO emissions from the four regions, consistent with the comparison of current global emission inventories by *Granier et al.* [2011].

[10] Previous publications based on the HTAP SR experiments have emphasized the effects of long-range transport on surface O_3, and other components, and comparisons with observations [*Sanderson et al.*, 2008; *Shindell et al.*, 2008; *Fiore et al.*, 2009; *Jonson et al.*, 2010; *Reidmiller et al.*, 2009]. *Fiore et al.* [2009] found that the HTAP ensemble mean surface O_3 concentrations compared well with observations over EU for the year 2001, but overestimated measurements by more than 10 ppb during the summer and fall over the eastern United States and Japan. *Jonson et al.* [2010] compared simulated vertical O_3 profiles with observed ozonesonde profiles, finding that the spread in CTM results (and their over and underestimation of O_3 soundings) increases in the spring and summer with more active chemistry. In the winter and spring, seasonal averages for most CTMs were within 20% of sonde measurements in the upper and middle troposphere. Simulated SO_4^{2-} concentrations at the surface for the base simulation (SR1) also have been compared to observations (M. Schulz, personal communication, 2011, preliminary results available at http://aerocom.met.no/cgi-bin/aerocom/surfobs_annualrs.pl), where the results show that the CTMs are generally realistic.

[11] Short-lived O_3 precursors affect tropospheric O_3 within hours to weeks after their emission; however, they also affect OH, which influences the lifetime of CH_4 and in turn, O_3 in the long term [*Prather*, 1996; *Wild et al.*, 2001; *Berntsen et al.*, 2005; *Naik et al.*, 2005]. Global CH_4 changes were calculated by *Fiore et al.* [2009], based on the CH_4 loss by tropospheric OH diagnostic reported for each CTM and SR3 through SR6, relative to the fixed CH_4 abundance of 1760 ppbv. Long-term O_3 responses are then calculated in each grid cell, following *West et al.* [2007, 2009b], by scaling the change in O_3 from the CH_4 control simulation (SR2 minus SR1) to the calculated global CH_4 change for

Table 2. Global CTMs Used for Multimodel Mean O_3, CH_4, and SO_4^{2-} Estimates

Model	Institution
CAMCHEM-3311m13[a]	NCAR, USA
FRSGCUCI-v01	Lancaster University, UK
GISS-PUCCINI-modelE	NASA GISS, USA
GMI-v02f	NASA GSFC, USA
INCA-vSSz	LSCE, France
LLNL-IMPACT-T5a[a]	LLNL, USA
MOZARTGFDL-v2[a]	GFDL, USA
MOZECH-v16	FZ Juelich, Germany
STOC-HadAM3-v01	University of Edinburgh, UK
TM5-JRC-cy2-ipcc-v1[a]	JRC, Italy
UM-CAM-v01	University of Cambridge, UK/NIWA, NZ

[a]The four global CTMs used for multimodel mean SO_4^{2-} estimates.

Table 3. Multimodel Mean ± 1 Standard Deviation Reductions in the Anthropogenic Emissions of NO_x, NMVOC, and CO (20% of Total Anthropogenic Emissions) Among the 11 HTAP CTMs Used Here[a]

Region	NO_x (Tg N a^{-1})	NMVOC (Tg C a^{-1})	CO (Tg a^{-1})
EA	1.17 ± 0.24 (0.20)	3.13 ± 1.24 (0.40)	25.58 ± 7.25 (0.28)
EU	1.48 ± 0.14 (0.09)	3.77 ± 1.88 (0.50)	15.40 ± 3.26 (0.21)
NA	1.48 ± 0.10 (0.07)	3.11 ± 1.34 (0.43)	19.69 ± 3.66 (0.19)
SA	0.46 ± 0.04 (0.09)	1.94 ± 0.63 (0.33)	15.82 ± 3.74 (0.24)

[a]Coefficient of variation (CV = standard deviation/mean) is in parentheses. Emissions for the individual CTMs are provided in Tables A2 and A3 of *Fiore et al.* [2009].

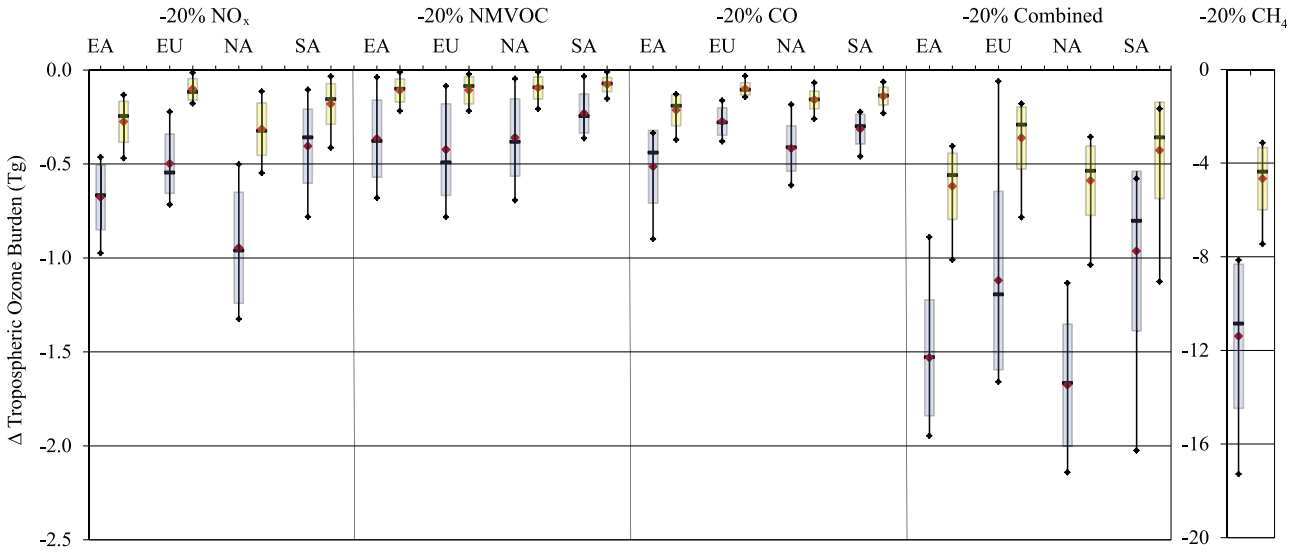

Figure 1. Global annual average changes in full (blue) and upper (yellow) tropospheric O_3 burden (Tg) at steady state (perturbation minus base), where the upper troposphere is from 500 hPa to the tropopause, for the HTAP ensemble of 11 models, showing the median (black bars), mean (red points), mean ± 1 SD (boxes), and max and min (whiskers), for each precursor reduction scenario (−20% global CH_4 burden, and −20% regional emissions of NO_x, NMVOC, CO, and combined from East Asia [EA], Europe and Northern Africa [EU], North America [NA], and South Asia [SA]).

each SR simulation and CTM. We then add the long-term O_3 responses to the simulated short-term O_3 responses to give O_3 concentrations at steady state.

[12] Since the HTAP CTMs were typically not designed to model stratospheric chemistry, we use the same three-dimensional monthly mean O_3 concentrations in the stratosphere and merge these with calculated steady state (short-term + long-term) tropospheric O_3 concentrations for each simulation and CTM. Stratospheric O_3 is taken for the year 2001 from the AC&C/SPARC O_3 database prepared for CMIP5 (Available: http://pcmdi-cmip.llnl.gov/cmip5/forcing.html). *Søvde et al.* [2011] found that around 15% of the RF from O_3 precursors is due to O_3 changes in the lower stratosphere, using a single model with both standard and updated chemistry. Since we ignore lower stratospheric O_3 changes, our RF estimates may underestimate the full effect of O_3 precursors. After each CTM's O_3 and SO_4^{2-} results are interpolated to a common resolution (longitude × latitude × level) as required by the RTM (72 × 37 × 33 for O_3; 96 × 80 × 14 for SO_4^{2-}), the HTAP ensemble mean ± 1 standard deviation O_3 and SO_4^{2-} distributions are calculated in each grid cell and month in three dimensions, in addition to the ensemble mean ± 1 standard deviation global CH_4 abundances (derived from the CH_4 loss by tropospheric OH diagnostics). Global O_3, CH_4, and SO_4^{2-} changes are calculated for each CTM as perturbation (SR2 to SR6) minus base (SR1) values.

2.2. GFDL Radiative Transfer Model

[13] We employ the GFDL RTM to estimate the net RF at steady state due to the changes in atmospheric gases (O_3 and CH_4) alone and due to combined changes in O_3, CH_4, and SO_4^{2-} aerosols. The GFDL RTM is a module of the GFDL coupled atmospheric-ocean model (AM2) and simulates solar and infrared radiative transfer [*GFDL GAMDT*, 2004; *Naik et al.*, 2005, 2007]. It has been used in studies of long-lived greenhouse gases [*Schwarzkopf and Ramaswamy*, 1999] and short-lived forcing agents such as O_3 and aerosols [*Naik et al.*, 2005, 2007; *West et al.*, 2007; *Fiore et al.*, 2008; *Saikawa et al.*, 2009]. Here the RTM is employed as for *Naik et al.* [2007] and *Saikawa et al.* [2009], at 144 × 90 × 24 levels, except for the following changes. We update well-mixed greenhouse gas concentrations based on observations for the year 2001 included as part of the historical period (1750–2005) of the CMIP5 Representative Concentration Pathways (RCP) database [*Meinshausen et al.*, 2011] (Available: http://www.iiasa.ac.at/web-apps/tnt/RcpDb/dsd?Action=htmlpage&page=download). We also update the solar data used by the RTM to the CMIP5 solar forcing data (Available: http://www.geo.fu-berlin.de/en/met/ag/strat/forschung/SOLARIS/Input_data/CMIP5_solar_irradiance.html). The RTM simulations do not include the indirect effects of aerosols on clouds or the internal mixing of aerosols. RF contributions from changes in nitrate aerosols, changes in stratospheric O_3 and water vapor, changes to the carbon cycle via O_3 and nitrogen deposition, and changes to CO_2 from CH_4, CO, and NMVOC oxidation are also omitted in the RTM simulations.

[14] The multimodel monthly mean ± 1 standard deviation O_3, CH_4, and SO_4^{2-} concentrations are used as input in the RTM simulations, along with meteorological fields from GFDL's atmosphere model (AM2) and land model (LM2), sampled one day per month at midmonth for the year 2001 to represent monthly mean conditions [*Naik et al.*, 2005]. Substantial variability in the SO_4^{2-} estimates across only four CTMs precluded evaluating the mean −1 standard deviation for SO_4^{2-} (e.g., several grid cells had standard deviations exceeding the mean). We simulate the monthly mean net radiation fluxes for the base and perturbed cases and calculate the net RF as the difference between the perturbed and

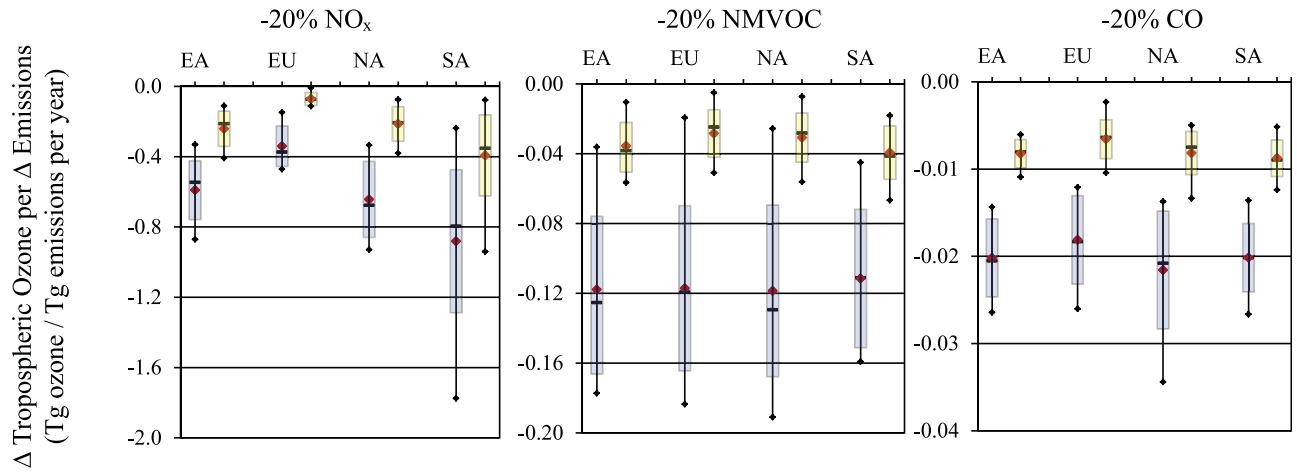

Figure 2. Global annual average changes in full (blue) and upper (yellow) tropospheric O_3 burden per change in emissions (Tg O_3/Tg emissions per year) at steady state for the individual 11 models, where the units of emissions are Tg N (for NO_x), Tg C (for NMVOCs), and Tg CO (for CO), showing the median (black bars), mean (red points), mean ± 1 SD (boxes), and max and min (whiskers) across the HTAP ensemble.

base net fluxes (net shortwave minus net longwave) at the tropopause, after allowing stratospheric temperatures to readjust to radiative equilibrium [*Naik et al.*, 2007; *Saikawa et al.*, 2009].

3. Tropospheric Composition Changes

3.1. Tropospheric Ozone Changes

[15] Figure 1 shows the changes in global annually averaged steady state tropospheric O_3 burden and its variability across 11 HTAP CTMs. Full troposphere and upper troposphere (UT) O_3 burdens are distinguished because O_3 in the UT has a higher RF efficiency on a per molecule basis [*Lacis et al.*, 1990; *Wang et al.*, 1993; *Forster and Shine*, 1997]. For each CTM's regridded O_3 distributions that have been blended with CMIP5 stratospheric O_3 values (section 2.1), the UT is defined from 500 hPa to the tropopause, where the tropopause is identified at the 150 ppbv O_3 level.

[16] The largest changes in full troposphere and UT O_3 burden are found for the 20% CH_4 reduction, followed by the 20% combined precursor reductions from NA and EA, respectively. However, there is considerable diversity among the 11 CTMs' estimates of full troposphere and UT O_3 burden changes. In these 17 SR simulations relative to the base case, the change in UT O_3 burden per change in full troposphere O_3 burden (UT O_3/full troposphere O_3) is largest for reductions in global CH_4 (0.36 to 0.47) and regional CO emissions (0.19 to 0.53), and smallest for regional NMVOC reductions (0.16 to 0.42) across the 11 CTMs, reflecting the longer lifetimes of CO and CH_4 in comparison to NMVOCs and NO_x. UT O_3/full troposphere O_3 is also largest for individual O_3 precursor (NO_x, NMVOC, and CO) reductions from SA in comparison to the other regions.

[17] To evaluate regional sensitivities, we consider how changes in full troposphere and UT O_3 burdens per unit change in emissions vary by region for each precursor (Figure 2). The CTMs mostly agree that the SA NO_x reduction produces the greatest change in full troposphere and UT O_3 burden per change in emissions out of the four regions, which can be attributed to more rapid vertical mixing, stronger photochemistry, and greater sensitivity of O_3 to precursor emissions from the tropics and southern hemisphere (SH) [*Kunhikrishnan et al.*, 2004; *West et al.*, 2009a]. We find less variability across the four regions in reducing full troposphere and UT O_3 burden per change in NMVOC and CO emissions (Figure 2), but six CTMs show that SA NMVOC and CO reductions produce the largest reductions in UT O_3 burden per change in emissions.

[18] For each regional reduction, the greatest changes in steady state tropospheric total column O_3 occur over the reduction region, in each individual CTM and across the HTAP ensemble (Figure 3). For NO_x reductions from each region, slight increases in O_3 burden occur in the SH, in contrast to overall decreases in the northern hemisphere (NH), due to long-term O_3 increases via CH_4 that are globally distributed (according to the pattern of O_3 response to CH_4) [*West et al.*, 2007, 2009b] (see section 3.2). As SA is further south than the other regions, the largest O_3 decreases occur near the tropics and do not extend as far north. The slightly higher increases in O_3 in the SH from the NA NO_x reduction correspond to this region producing greater increases in global CH_4 (Figure 4). For NMVOC and CO reductions from the four regions, we find decreases in total column O_3 in both the SH and NH, as sustained decreases in these precursors cause both short- and long-term global O_3 decreases. NMVOC reductions also reduce global annual average peroxy acetyl nitrate (PAN) burdens from the four regions by 1.4 ± 0.6% (SR4EA), 2.0 ± 0.8% (SR4EU), 1.5 ± 0.5% (SR4NA), and 0.5 ± 0.2% (SR4SA), relative to the base, through which NMVOCs can influence the nitrogen cycle and therefore long-range O_3. Across the 11 CTMs, we find that tropospheric PAN decreases are correlated to the changes in NMVOC emissions for the EA, EU, and NA reductions.

3.2. Tropospheric Methane Changes

[19] Although global CH_4 was held constant by each CTM in all perturbations, we analyze the changes in global

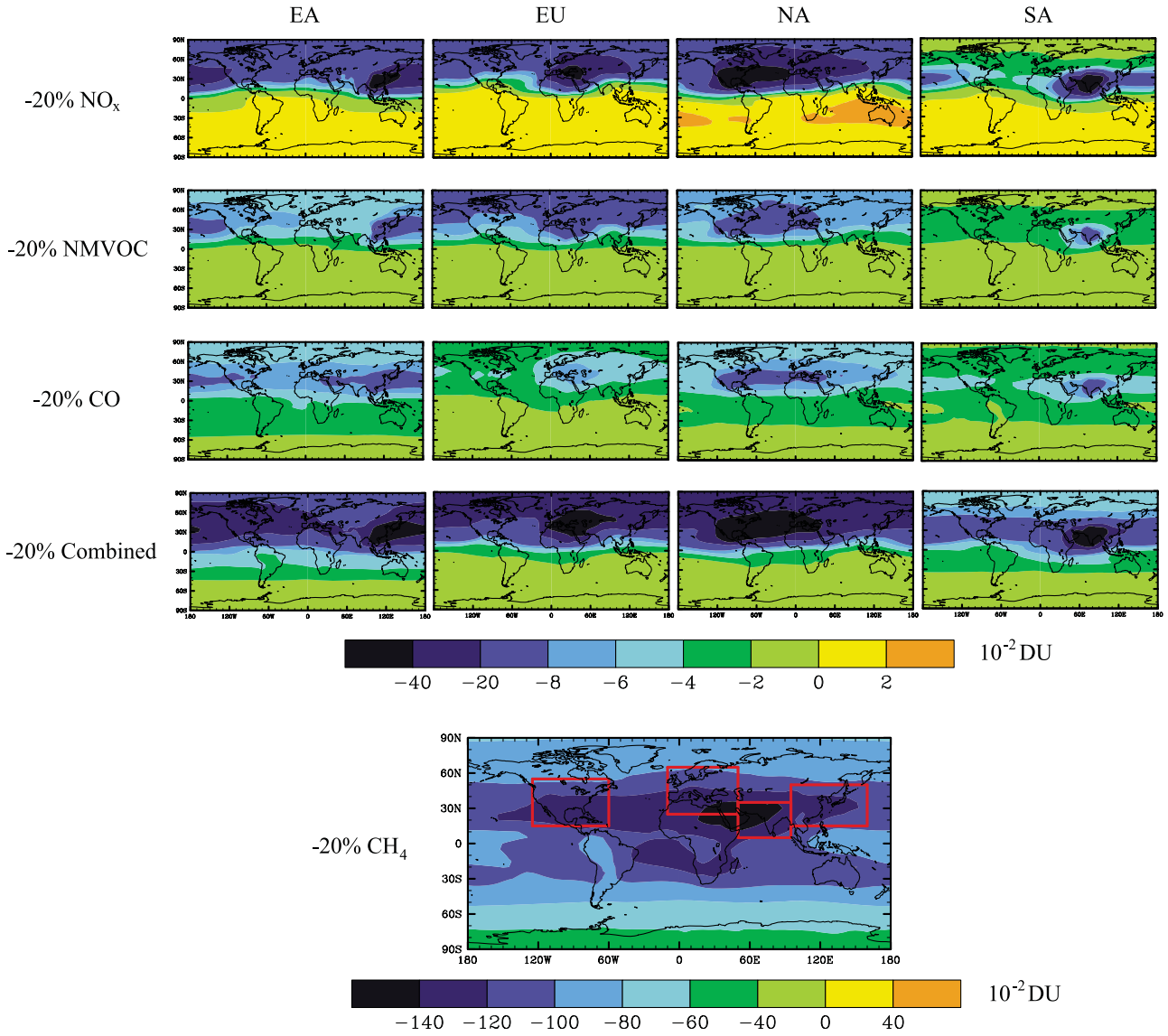

Figure 3. Annual average steady state tropospheric total column O_3 burden changes (10^{-2} DU) for the multimodel mean of 11 HTAP models, for each of the precursor reduction scenarios (−20% CH_4 burden, and −20% regional emissions of NO_x, NMVOC, CO, and combined). The 4 regions of reduction (NA, EU, SA, EA) are outlined in red in the −20% CH_4 plot.

tropospheric CH_4 calculated off-line for each perturbation. NO_x reductions from all four regions increase global CH_4 abundance via decreases in OH, while NMVOC and CO reductions from all four regions decrease global CH_4 (Figure 4). These changes in CH_4 drive the long-term O_3 changes discussed in the previous section. For particular precursors, reductions from certain regions, e.g., CO reductions from EA, are slightly more effective at decreasing global CH_4 than other regions. However, there is noticeable variability among the CTMs' changes in global CH_4 (Figure 4), which is partly explained by variance in CTM emissions for CO, but not for NO_x and NMVOCs.

[20] For several CTMs, some emissions perturbations had minimal impact on global OH, resulting in calculated steady state CH_4 changes of zero. In addition, the CVs of CH_4 change are lowest in magnitude for NO_x reductions (0.22 to 0.39) and highest for NMVOC reductions (−0.40 to −1.12), perhaps reflecting differing NMVOC speciation and chemical schemes among the CTMs [*Collins et al.*, 2002].

[21] We compare the change in global CH_4 from the combined precursor reductions to the sum of global CH_4 changes from NO_x, NMVOC, and CO reductions to assess the additivity of individual precursor reductions on global CH_4. Based on the HTAP multimodel mean results, global CH_4 changes from SA and NA combined precursor reductions are approximately 59% and 75%, respectively, of the sum of CH_4 changes from individual precursor reductions, while global CH_4 changes from EA and EU combined precursor reductions are slightly negative in contrast to small positive global CH_4 changes from the sum. The three (of 11) CTMs that did not include reductions in SO_2 and aerosols in the SR6 experiments [*Fiore et al.*, 2009] show global CH_4

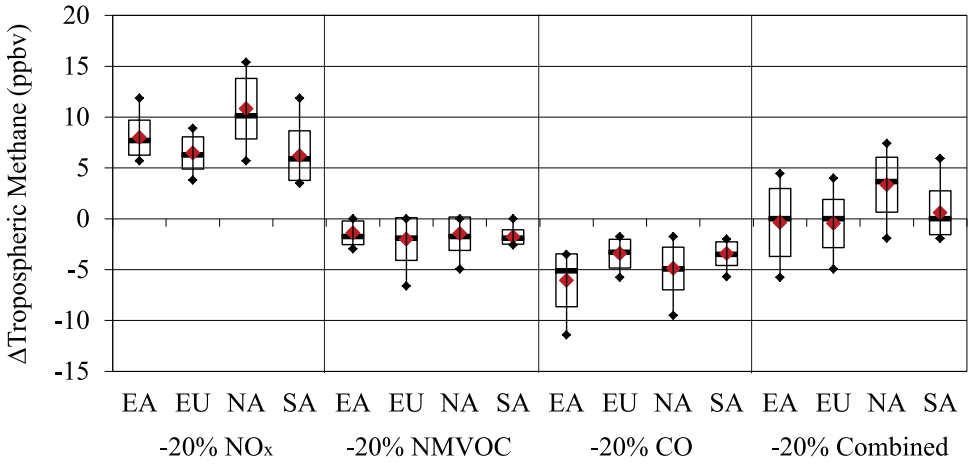

Figure 4. Global annual multimodel changes (perturbation minus 1760 ppbv) in tropospheric CH_4 (ppbv) for −20% regional emissions of NO_x, NMVOC, CO, and combined: median (black bars), mean (red points), mean ± 1 SD (boxes), and max and min (whiskers) for the HTAP ensemble of 11 models, estimated directly from the CH_4 loss by tropospheric OH archived by each HTAP CTM [*Fiore et al.*, 2009]. Tropospheric CH_4 changes were not available from INCA-vSSz for SA 20% NMVOC reduction and from LLNL-IMPACT-T5a for 20% NO_x reductions (EA, EU, NA, SA); these models are excluded from the multimodel CH_4 changes for these perturbations.

changes from the combined precursor reductions close to the sum of CH_4 changes from individual NO_x, NMVOC, and CO reductions. This suggests that deviations from additivity may be due to reductions in SO_2 and aerosols (in SR6) affecting CH_4.

3.3. Tropospheric Sulfate Changes

[22] There is considerable variability and disagreement in the sign of SO_4^{2-} responses among the four CTMs evaluated (Figure 5). The greatest variability in global SO_4^{2-} burden across the CTMs occurs for the CH_4 reduction and for NO_x reductions from all four regions. There is less variability across CTMs for NMVOC and CO reductions, but still differences in the sign of change.

[23] The four CTMs analyzed here account for SO_4^{2-} formation through two main oxidation pathways: 1) gas-phase oxidation of sulfur dioxide (SO_2) by OH, and 2) aqueous-phase oxidation of SO_2 by H_2O_2 or O_3 [*Houweling et al.*, 1998; *Jeuken et al.*, 1999, 2001; *Barth et al.*, 2000; *Rasch et al.*, 2000; *Horowitz et al.*, 2003; *Rotman et al.*, 2004; *Tie et al.*, 2005]. Since CH_4, NMVOC, and CO reductions increase OH concentrations, SO_2 oxidation via pathway (1) is expected to increase tropospheric SO_4^{2-} formation. At the same time, increases in H_2O_2 (occurring with increases in OH) are expected to increase SO_2 oxidation via pathway (2), but decreases in O_3 may decrease oxidation (also pathway (2)). NO_x reductions not only decrease O_3, but can also decrease OH and H_2O_2, which leads to decreases in

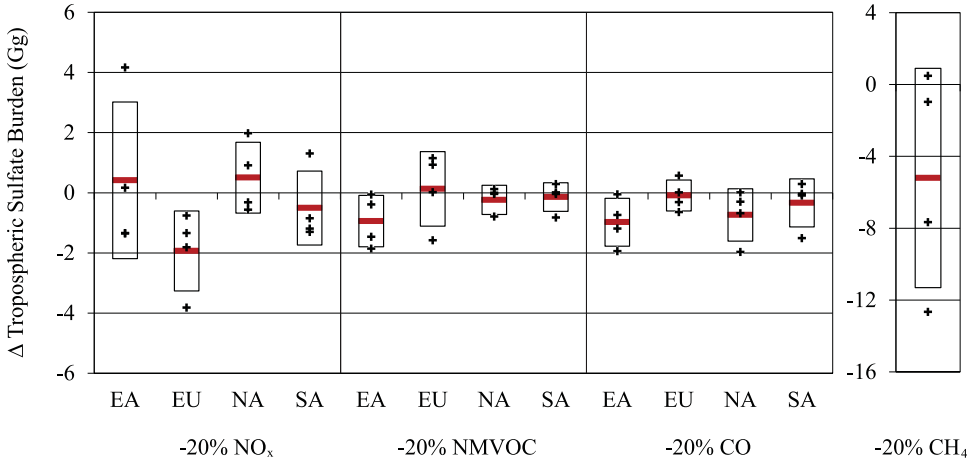

Figure 5. Global annual multimodel changes (perturbation minus base) in short-term tropospheric SO_4^{2-} (Gg) for −20% CH_4 burden and −20% regional emissions of NO_x, NMVOC, and CO: mean (red bars) and mean ± 1 SD (boxes) across the HTAP ensemble of four models. The individual model results are shown in black (pluses).

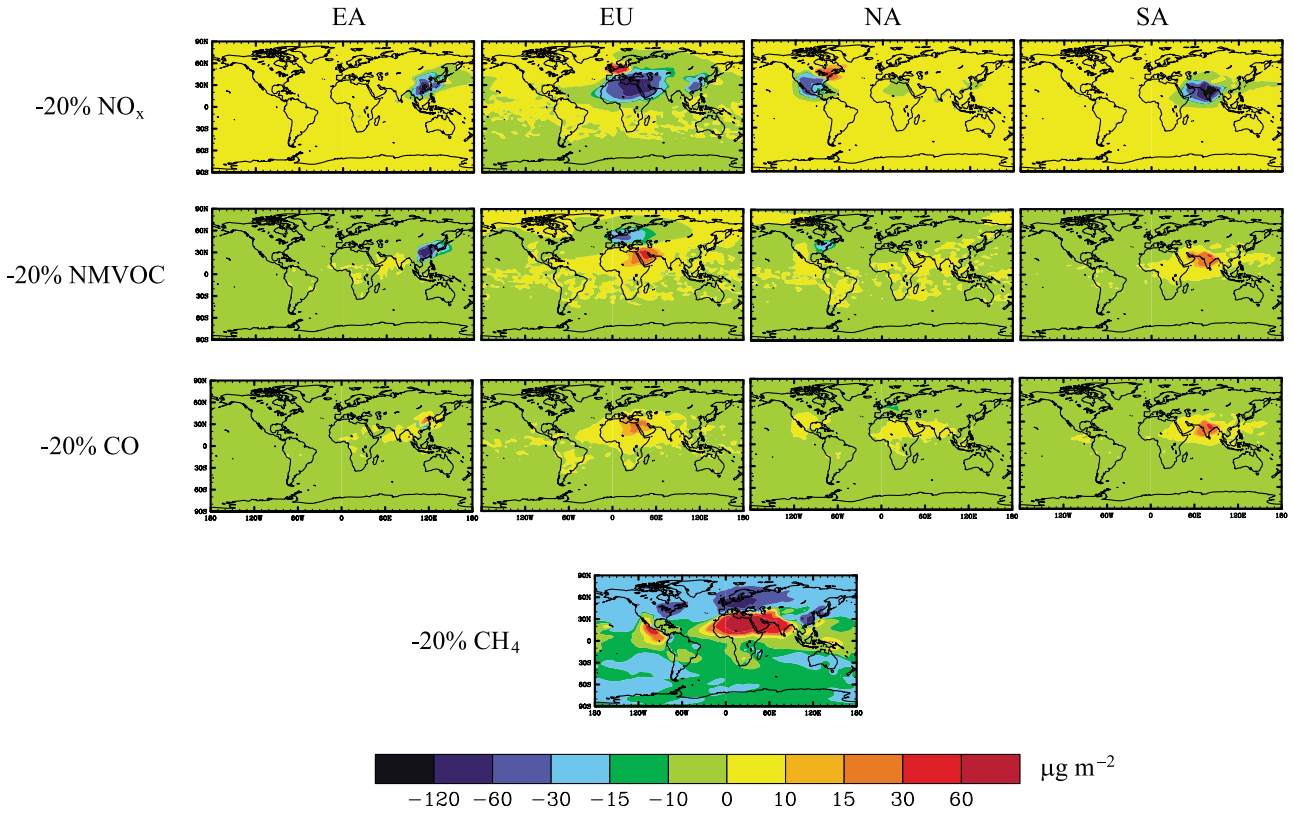

Figure 6. Annual average tropospheric total column SO_4^{2-} burden changes ($\mu g\ m^{-2}$) for the multimodel mean of four HTAP models for −20% CH_4 burden and −20% regional emissions of NO_x, NMVOC, and CO scenarios.

SO_4^{2-} formation by pathways (1) and (2). Figure 5 shows that the sign of SO_4^{2-} response is not consistent across all four CTMs, suggesting uncertainty in the modeled effects of O_3 precursors on oxidants, the relative importance of these oxidation pathways, and the lifetime and removal of SO_2 and SO_4^{2-}.

[24] The global distributions of tropospheric total column SO_4^{2-} changes (Figure 6) show the greatest changes in SO_4^{2-} over the region of emission change, with only slight changes globally. The individual CTMs and HTAP ensemble mean results show that NO_x reductions from EA, EU, and NA cause both increases and decreases in SO_4^{2-} over the reduction region, which correspond to changes in oxidants (OH, H_2O_2, O_3); localized decreases in SO_4^{2-} are due in part, to localized decreases in OH (auxiliary material Figure S5) and decreases in O_3.[1] The distributions of H_2O_2 are not analyzed, as they were not reported in the CTM simulations. NMVOC reductions from EU increase SO_4^{2-} over northeastern Africa and decrease SO_4^{2-} over western Europe in three of the CTMs and the ensemble mean. All four CTMs consistently show that the EA NMVOC reduction decreases SO_4^{2-} and the SA NMVOC reduction increases SO_4^{2-} regionally, while two CTMs show SO_4^{2-} decreases over the eastern U.S. from the NA NMVOC reduction. For CO reductions from all four regions, the ensemble mean shows localized increases, while the individual CTMs differ in the sign of regional SO_4^{2-} change for all CO reductions except SA. Regional increases in SO_4^{2-} from the NMVOC and CO reductions can be explained partly by localized increases in OH (Figure S5); however, decreases in SO_4^{2-} may be related to the differing effects on oxidants (including H_2O_2) and on the SO_2 oxidation pathways in each CTM, as discussed in the previous paragraph.

4. Radiative Forcing due to Precursor Emission Changes

[25] Figure 7 (and Table S1 in auxiliary material Text S1) show the global annual net RF due to O_3, CH_4, and SO_4^{2-}, estimated from RTM simulations, first for multimodel mean O_3 and CH_4, and second for multimodel mean O_3, CH_4, and SO_4^{2-}, for each SR scenario relative to the base case. We calculated the net RF distributions for each perturbation scenario (SR2 through SR6) by subtracting (in each grid cell and month) the simulated radiative fluxes for the base case (SR1) from those for each perturbation. To estimate the contribution of the multimodel mean SO_4^{2-} to the global annual net RF, we subtracted the net RF results due to O_3 and CH_4 from the net RF due to O_3, CH_4, and SO_4^{2-} for each SR scenario, assuming the effects of O_3, CH_4, and SO_4^{2-} are additive. To distinguish the contributions of O_3 and CH_4 to the global annual net RF, we estimated the net RF due to the multimodel mean CH_4 for each SR scenario, using the formula of *Ramaswamy et al.* [2001], attributing the difference to O_3 RF.

[1] Auxiliary materials are available in the HTML. doi:10.1029/2011JD017134.

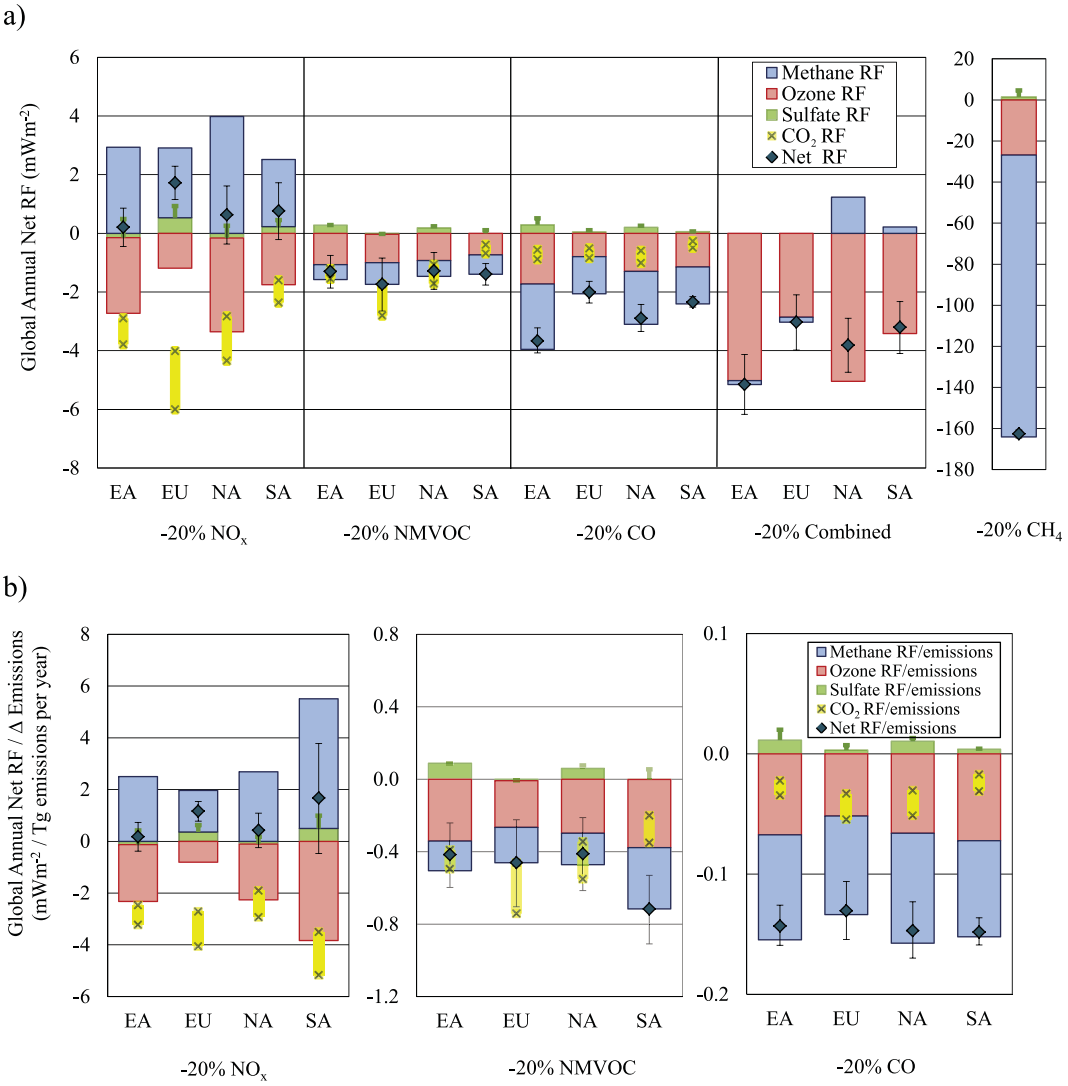

Figure 7. (a) Global annual average RF (mW m^{-2}) for the HTAP ensembles of 11 models (for O_3 and CH_4 forcing) and four models (for SO_4^{2-} forcing) due to multimodel mean changes in steady state O_3, CH_4, and SO_4^{2-}. Vertical black bars represent the uncertainty in net RF across models, calculated as the net RF of the multimodel mean ± 1 standard deviation O_3 and CH_4, for each perturbation (−20% CH_4 burden, and −20% regional emissions of NO_x, NMVOC, CO, and combined), relative to the base simulation. The uncertainty estimates for −20% CH_4 account only for the variability in simulated O_3 changes across the CTMs, since all CTMs uniformly reduced CH_4 (1760 ppbv to 1408 ppbv). Vertical green bars represent the upper uncertainty bound of SO_4^{2-} RF across models, calculated as the net RF of the multimodel mean +1 standard deviation SO_4^{2-}. The RF of changes in CO_2 uptake by the biosphere (yellow) are shown as a range from high to low sensitivity of vegetation to O_3, estimated for a single CTM (STOCHEM) by *Collins et al.* [2010]; these estimates are not included in the net RF (supporting data provided in Table S1 in auxiliary material Text S1). Note the difference in scale between the −20% regional (NO_x, NMVOC, CO, combined) and −20% CH_4 reduction scenarios. (b) Global, annual average RF per multimodel mean change in emissions (mW m^{-2}/Tg emissions per year) due to multimodel mean changes in steady state O_3, CH_4, and SO_4^{2-}, and uncertainty (vertical black bars) as the net RF of the multimodel mean ± 1 standard deviation changes in O_3 and CH_4 per unit change in emissions for each perturbation, relative to the base simulation. Vertical green bars represent the upper uncertainty bound of SO_4^{2-} RF per unit change in emissions across models.

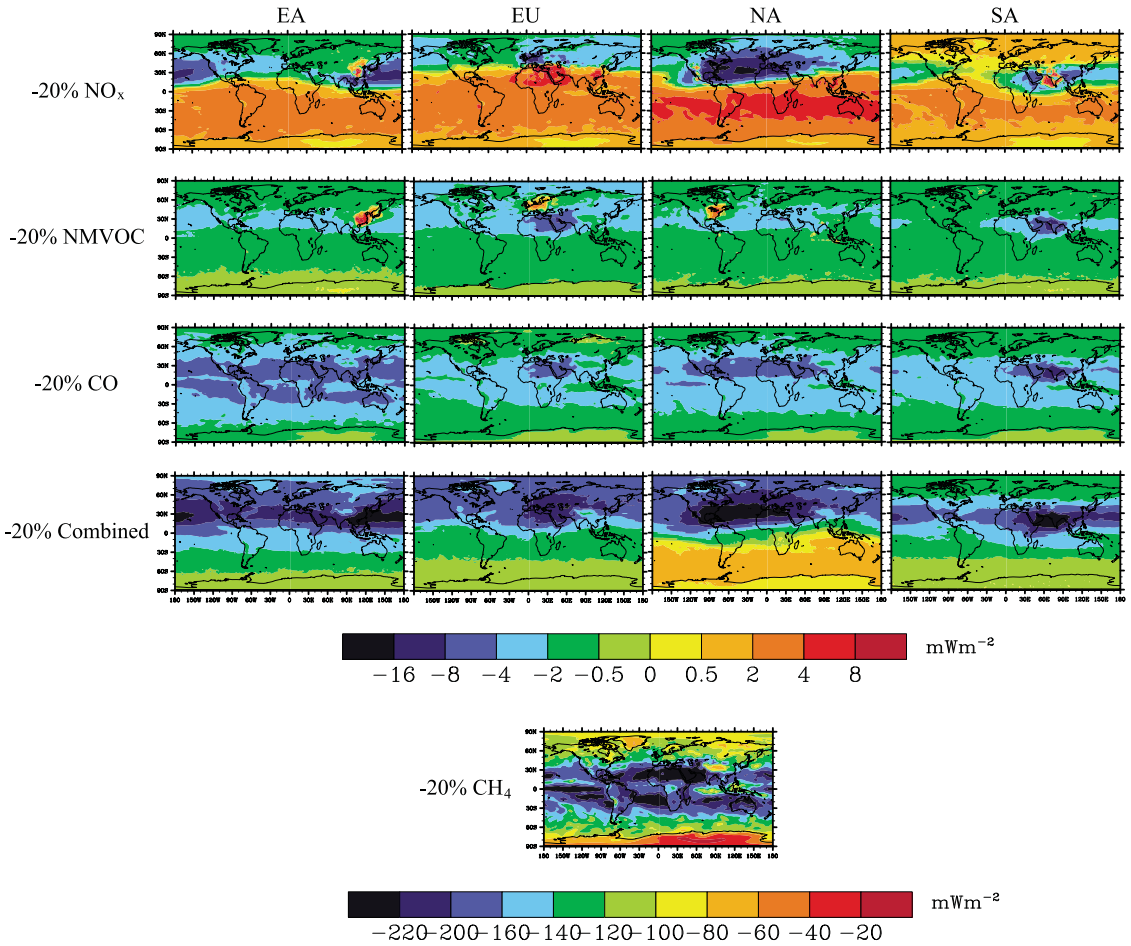

Figure 8. Annual average net RF distributions (mW m^{-2}), calculated as the annual shortwave radiation minus the annual longwave radiation, due to tropospheric O_3, CH_4, and SO_4^{2-} for the multimodel mean, for each of the precursor reduction simulations (−20% CH_4 burden and −20% regional emissions of NO_x, NMVOC, CO, and combined) minus the base simulation. Note the difference in scale between the −20% regional (NO_x, NMVOC, CO, combined) and −20% CH_4 reduction scenarios.

[26] Computational limitations prevented us from simulating the RFs individually for each CTM's 18 SR scenarios. Instead, we simulate RFs for multimodel means, and for the multimodel mean ± 1 standard deviation O_3 and CH_4 and the multimodel mean +1 standard deviation SO_4^{2-} to account for uncertainty in the net RF due to differences in the CTMs. We show uncertainty (mean ± 1 standard deviation) for the resulting net RF, which includes the uncertainty in O_3 and CH_4 RFs, as changes in O_3 and CH_4 are not strongly correlated among the 11 CTMs for most scenarios (Figure S4). For NO_x reductions, because the RF due to O_3 opposes that of CH_4, a broader uncertainty range would have resulted had we instead simulated together the multimodel mean +1 standard deviation O_3 and the multimodel mean −1 standard deviation CH_4 (and the reverse) to estimate uncertainty.

[27] Figure 7 shows that O_3 and CH_4 RFs have the same sign as the tropospheric composition changes in section 3; since SO_4^{2-} is cooling, SO_4^{2-} RF has the opposite sign. NO_x reductions from all four regions produce an overall positive net RF due to increases in CH_4, which outweigh the negative net RF due to decreases in O_3 (Figure 7a). Negative global net RFs are produced by CO and NMVOC reductions, due to O_3 and CH_4 decreases, and also by the combined precursor reductions, as increases in CH_4 from NO_x reductions roughly cancel CH_4 decreases from NMVOC and CO reductions [*Fiore et al.*, 2009]. The net RF due to the combined precursor reduction is 98% to 117% of the sum of the net RFs (of O_3 and CH_4) due to reductions of each individual precursor, across the four regions, showing approximate additivity for the different precursors.

[28] Consistent with the SO_4^{2-} changes in Figure 5, NO_x reductions from EU and SA contribute a positive SO_4^{2-} RF, while EA and NA NO_x reductions produce negative SO_4^{2-} RF. The SO_4^{2-} RFs for NMVOC and CO reductions vary in magnitude and sign across the four regions, corresponding to the disagreement in SO_4^{2-} response across the CTMs (Figure 5). We do not estimate the contribution of SO_4^{2-} to net RF for the combined reductions, since many of these perturbations included 20% reductions in SO_2 and aerosols, making it difficult to isolate the effect of NO_x, NMVOC, and CO on SO_4^{2-} RF.

[29] Figure 7 also shows an estimate of the RF due to the CO_2 equivalent emission resulting from the influence of surface O_3 on plants' ability to remove CO_2 from the

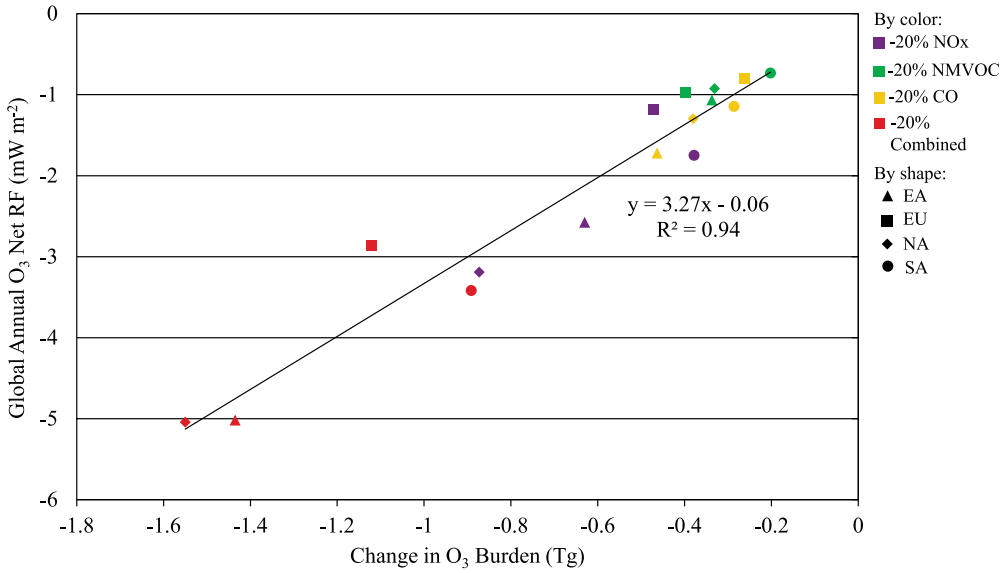

Figure 9. Radiative forcing efficiency of O_3 for the 16 SR simulations (SR3 through SR6) for the multi-model mean, showing the global, annual average O_3 net RF (mW m^{-2}), calculated as the difference between the simulated net RF due to O_3 and CH_4 and estimated net RF due to CH_4 [*Ramaswamy et al.*, 2001], versus the global, annual average steady state changes in tropospheric O_3 burden (Tg). The SR simulations are distinguished by precursor (color) and region (shape).

atmosphere, from *Collins et al.* [2010], based on one HTAP CTM (STOCHEM) and not the HTAP ensemble. The CO_2 responses to pulse changes from *Collins et al.* [2010] were converted to equilibrium responses by integrating over 100 years. The range of CO_2 RF represents high to low sensitivity of vegetation to O_3. With the additional consideration of CO_2 RF, the global annual net RF due to regional NO_x reductions changes sign to an overall net climate cooling (-0.83 to -4.28 mWm^{-2} for all four regions), while the negative net RFs for regional NMVOC and CO reductions are reinforced by the addition of CO_2 RF (Table S1 in auxiliary material Text S1).

[30] We normalize the global annual net RF estimates (Figure 7a) by each region's reduction in emissions (Table 3). The net RF per unit change in NO_x and NMVOC emissions is greatest for SA reductions out of the four regions (Figure 7b), corresponding to the sensitivity findings in section 3.1. For CO reductions, all four regions are approximately as effective at reducing global net RF per unit CO emissions, consistent with CO's longer atmospheric lifetime.

[31] We compare our ensemble mean global annual net RF estimates per unit NO_x emissions to those of *Naik et al.* [2005], who used a single CTM and analyzed 10% NO_x reductions. Our estimates are approximately 32% to 63% (EU, NA, SA) and 16% (EA) of those reported by *Naik et al.* [2005], but these differences in net RF (CH_4 and O_3 RF combined) are small in comparison to the magnitudes of CH_4 and O_3 forcing individually.

[32] The net RF distributions (Figure 8) correspond to the distributions of total column O_3 (Figure 3) and SO_4^{2-} changes (Figure 6), where regional to hemispheric RF corresponds to O_3 changes and more localized RF is dominated by SO_4^{2-} changes, as illustrated by shortwave forcings (Figure S2). Changes in CH_4 influence net RF globally, since a uniform CH_4 mixing ratio was specified in each RTM simulation. For NO_x reductions, we find positive net RFs in the SH due to CH_4 and long-term O_3 increases globally, but in the NH these positive RFs are outweighed by the negative RF of O_3 decreases (Figure 8). For CH_4, NMVOC, CO, and combined reductions, negative net RFs from O_3 decreases in the NH overlay negative RFs globally due to CH_4. While Figure 7 presents globally averaged forcings, the regionally inhomogeneous forcings in Figure 8 are also relevant for regional climate change [*Shindell and Faluvegi*, 2009]. However, regional RF patterns resulting from changes in tropospheric loadings do not directly translate to regional climate responses [*Levy et al.*, 2008; *Shindell et al.*, 2010].

[33] In Figure 9, the relationship between tropospheric O_3 burden changes and global O_3 RF is strongly linear, giving a RF efficiency of approximately 3.27 mW m^{-2} per Tg O_3 or 35.6 mWm^{-2} DU^{-1} (1 DU $\approx$ 10.88 Tg O_3 [*Park et al.*, 1999]). This efficiency compares well with those estimated in previous studies, 34 to 48 mWm^{-2} DU^{-1} [*Hauglustaine and Brasseur*, 2001; *Wild et al.*, 2001; *Fiore et al.*, 2002] and 23 mWm^{-2} DU^{-1} (for NO_x) and 43 mWm^{-2} DU^{-1} (for CH_4 and CO+VOCs) [*Shindell et al.*, 2005]. Here reductions from EU and NA (with exception of NA NO_x) fall at or above the average RF efficiency line, suggesting lower RF efficiency. EA and SA reductions (except for EA NMVOC) have RF efficiency greater than average, as these regions have greater influences on the UT where RF is the most efficient [*Lacis et al.*, 1990; *Wang et al.*, 1993; *Forster and Shine*, 1997; *West et al.*, 2009a].

5. Global Warming Potentials

[34] Beyond analyzing RF, the climate impacts of O_3 precursor emissions can be compared with each other, and

with the emissions of other species using climate metrics such as the global warming potential (GWP). *Forster et al.* [2007] suggest that there are serious limitations to the use of GWPs for comparing short-lived species. While other metrics have been proposed to compare climate effects, such as the global temperature potential (GTP) [*Shine et al.*, 2005, 2007], none are as widely used as the GWP. We choose to analyze the GWP here for comparison with earlier studies.

[35] The basis for the GWP calculation is the integrated RF following a pulse emission. In section 4, O_3 RF was calculated for equilibrium conditions for the sum of the short and long-term O_3 responses (Figure 7, and Table S1 in auxiliary material Text S1). Here long-term O_3 RF is calculated by scaling O_3 RF from SR2 by the ratio of steady state O_3 burden change in a particular SR scenario (SR minus base) to those of SR2 (SR2 minus base). The short-term O_3 RF is then the difference between the steady state RF (section 4) and long-term RF. Following *Collins et al.* [2010], RF as a function of time is calculated for a one-year emissions perturbation, for each SR scenario. The short-term RF components (SO_4^{2-} and short-term O_3) are assumed to be constant over the one-year pulse and then drop to zero instantaneously; whereas, the long-term components (CH_4 and long-term O_3) respond and decay with the multimodel mean CH_4 perturbation lifetime (11.65 years). For the 20% CH_4 reduction (SR2), an analytical expression is used to calculate the impact of a one-year emissions pulse and subsequent decay [*Collins et al.*, 2010]. This CH_4 perturbation is used to scale the SO_4^{2-} and O_3 RFs from SR2 in Figure 7. The formula by *Ramaswamy et al.* [2001] is used to calculate the CH_4 RF.

[36] GWP_H is given by the RF integrated out to a time horizon H and normalized by the change in emissions, divided by the equivalent for CO_2. In Figure 10, and Table S2 in auxiliary material Text S1, we present GWPs for the 20- and 100-year time horizons (GWP_{20} and GWP_{100}). The uncertainties are dominated by the variation in CH_4 response across the CTMs. For NO_x emissions, this uncertainty is sufficiently large that it is not possible to identify the sign of the GWPs. The patterns of GWP_{100} are very similar to the normalized forcings in Figure 7b (the patterns would be identical for GWP_∞), whereas the GWP_{20} patterns give more emphasis to short-lived O_3 and SO_4^{2-} than GWP_{100}. For NO_x emissions, this brings GWP_{20} proportionally closer to zero.

[37] For NO_x reductions, the GWP_{100} estimates are similar to those of *Forster et al.* [2007] and *Fuglestvedt et al.* [2010], though substantially smaller than those provided by *Shindell et al.* [2009]. The O_3 contribution from Asian NO_x found by *Berntsen et al.* [2005] is within the range of the HTAP CTMs' results, but slightly higher than the HTAP multimodel mean. We neglect RFs of nitrate aerosols, but *Bauer et al.* [2007] suggest nitrate contributions to NO_x GWPs on the order of -80 for GWP_{20} and -20 for GWP_{100}. The NMVOC GWPs (Figure 10) are generally smaller than those of *Collins et al.* [2002]; however, *Collins et al.* [2002] covered a range of individual NMVOCs. For CO, the GWPs are comparable to those of *Derwent et al.* [2001], but smaller than those of *Berntsen et al.* [2005], largely due to the lower O_3 response of the HTAP multimodel mean; the O_3 response to Asian CO emissions of *Berntsen et al.* [2005], however, is within the range of the HTAP CTMs. The CO GWP_{100} estimates are also smaller than the no-aerosol results of *Shindell et al.* [2009], due to a lower CH_4 response. The O_3 contribution to GWP_{100} for CH_4 is smaller in this multimodel study (21% of the direct CH_4 contribution) than the 25% assumed by *Forster et al.* [2007], mostly because changes in O_3 above the tropopause are neglected. Adding in the contribution of O_3 in the lower stratosphere (15% of O_3 RF) [*Søvde et al.*, 2011], and that for stratospheric water vapor (15% of the CH_4 contribution) would give a total GWP_{100} for CH_4 of 24.2 ± 4.2.

[38] For NO_x and NMVOCs, SA emissions have a larger impact than emissions from the other regions. This suggests that some latitudinal dependence may be appropriate for GWPs of O_3 precursors. Note that equatorial or SH emission changes were not considered in this study, but *Fuglestvedt et al.* [2010] found a dependence on latitude. European NO_x emissions have a more negative GWP than other regions in the northern midlatitudes, as O_3 production in this NO_x-saturated region is lower.

6. Conclusions

[39] We quantify the magnitude and distribution of global net RF due to changes in O_3, CH_4, and SO_4^{2-} for 20% reductions in global CH_4 and regional NO_x, NMVOC, CO, and combined precursor emissions. We find that the 20% NO_x reductions produce global, annually averaged positive net RFs, as positive CH_4 RFs outweigh negative O_3 RFs, consistent with previous studies [*Fuglestvedt et al.*, 1999; *Wild et al.*, 2001; *Naik et al.*, 2005; *West et al.*, 2007]. For CH_4, NMVOC, and CO reductions, O_3 and CH_4 RFs are synergistic, yielding overall negative net RFs, consistent with previous global-scale studies [*Fiore et al.*, 2002; *West et al.*, 2007; *Shindell et al.*, 2009]. Including the effects of O_3 on plant growth and the carbon cycle may change the sign of net RF for NO_x reductions to an overall net climate cooling, in contrast to previous results that neglect this effect, while reinforcing the negative net RFs due to NMVOC and CO reductions, but future research is needed to better quantify this effect.

[40] By normalizing the net RF estimates by changes in emissions (for NO_x, NMVOC, and CO), we find that RF is more sensitive to NO_x and NMVOC emission reductions from regions closer to the equator (i.e., SA), consistent with our findings that changes in O_3 burden per change in emissions (full troposphere and UT O_3 for NO_x, and UT O_3 for NMVOC) are greatest for SA reductions. RF is more uniformly sensitive to CO emission reductions from each of the four regions, which agrees with O_3 burden changes per unit CO being less variable across the four regions. The trends in GWP_{100} across the four regions, for each precursor, reflect the normalized net RF results. Compared to GWP_{100}, the GWP_{20} patterns are influenced more by short-term O_3 and SO_4^{2-}. The large uncertainties in the NO_x GWP estimates, mainly from the variation in calculated CH_4 responses across the CTMs, limit the determination of the sign of NO_x GWPs. The estimated GWPs for individual regions are from the largest model ensemble that has been analyzed to date, and are broadly comparable to previous studies.

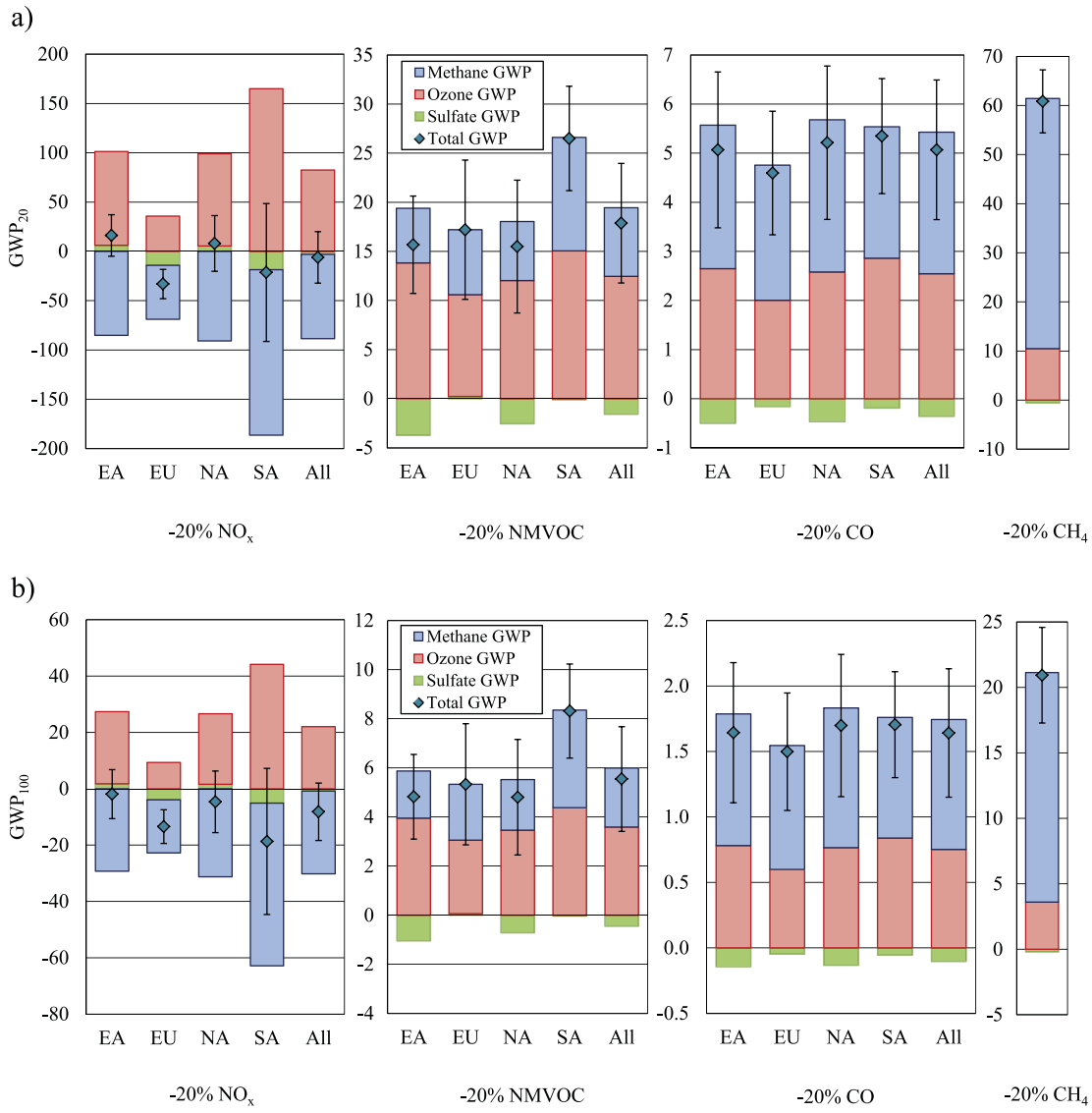

Figure 10. GWPs for time horizons of (a) 20 years and (b) 100 years for the −20% CH_4 burden and −20% regional emissions of NO_x, NMVOC, and CO scenarios. The four regions' estimates (labeled "All") represent the GWP due to the sum of the four regions' responses (to O_3, CH_4, SO_4^{2-}, and all three species [Total GWP]). Uncertainty analysis is as in Figure 7, but also includes the uncertainty in the CH_4 lifetimes for the base simulation (SR1) (supporting data available in Table S2 in auxiliary material Text S1).

[41] We find that regional RFs correspond to localized increases and decreases in SO_4^{2-} burden. O_3 changes are most important for RF on the regional to hemispheric scales, and CH_4 influences RF globally, dominating the RF response in the SH. The estimated contribution of SO_4^{2-} (direct effect only) to net RF is small compared to the RF of O_3 and CH_4. *Shindell et al.* [2009] found with a single CTM that for global NO_x, CO, and VOC emissions, changes in SO_4^{2-} contributed a RF more comparable in magnitude to the RFs of O_3 and CH_4. Our findings contrast with those of *Shindell et al.* [2009] on the importance of SO_4^{2-} RF due to O_3 precursors. However, the robustness of these results is limited, since there was substantial variability in SO_4^{2-} among only four HTAP CTMs. The effects of O_3 precursors on SO_4^{2-} via oxidants merit further research, using newer models that include improved treatment of oxidant-aerosol interactions.

[42] We account for variability in O_3, CH_4, and SO_4^{2-} across the ensemble of CTMs, but our estimates of uncertainty only include the variability in CTMs, using a single RTM for all RF estimates. We therefore understate the uncertainty in net RF. In addition, while we capture the most important forcings, a more complete analysis of RF could include RFs due to changes in nitrate aerosols (likely important for NO_x reductions), the indirect effect of aerosols, internal mixing of aerosols, changes in stratospheric O_3

and water vapor, and changes to the carbon cycle via nitrogen deposition. Finally, we estimate RF due to changes in the radiative budget of the global atmosphere, but do not estimate the full climate response to regional forcings. Future research should link global and regional RF to climate responses.

[43] Our analysis contributes to the understanding of the effects of O_3 precursors on global and regional RF, and provides motivation for evaluating the climate benefits of policies addressing tropospheric O_3 and its precursors. We show that among short-lived O_3 precursors, NMVOC and CO emission reductions most effectively reduce RF. Our GWP estimates could form the basis for regionally specific GWPs (or comparable metrics), which may allow O_3 precursors to be included in future climate agreements and emissions trading schemes, as well as provide information that could be used to estimate the influence of national or regional policies. Variability in GWPs among regions for NO_x and NMVOCs suggests that regionally specific estimates would be important. For CO, the consistency in RF per unit emissions and GWP_{100} across the four regions implies that the error in using a uniform GWP for CO may be small. However, the RF per unit CO emissions may differ in other regions not studied here. Future studies should analyze additional source regions, such as near the equator and in the SH, as other precursors show greater sensitivity in these regions [e.g., *Naik et al.*, 2005].

[44] **Acknowledgments.** The research described in this paper has been funded wholly or in part by the United States Environmental Protection Agency (EPA) under the Science to Achieve Results (STAR) Graduate Fellowship Program (to M.M. Fry), by the EPA Office of Air Quality Planning and Standards, and by a UNC Junior Faculty Development award (to J.J. West). EPA has not officially endorsed this publication, and the views expressed herein may not reflect the views of the EPA. W.J. Collins was supported by the Joint DECC/Defra Met Office Hadley Centre Climate Programme (GA01101) and Defra contract AQ0902. We thank those involved in the CTM simulations performed under the UN ECE Task Force on Hemispheric Transport of Air Pollution. The NOAA Geophysical Fluid Dynamics Laboratory provided the necessary computational resources.

References

Barth, M. C., P. J. Rasch, J. T. Kiehl, C. M. Benkovitz, and S. E. Schwartz (2000), Sulfur chemistry in the National Center for Atmospheric Research Community Climate Model: Description, evaluation, features, and sensitivity to aqueous chemistry, *J. Geophys. Res.*, *105*(D1), 1387–1415, doi:10.1029/1999JD900773.

Bauer, S. E., D. Koch, N. Unger, S. M. Metzger, D. T. Shindell, and D. G. Streets (2007), Nitrate aerosols today and in 2030: A global simulation including aerosols and tropospheric ozone, *Atmos. Chem. Phys.*, *7*, 5043–5059, doi:10.5194/acp-7-5043-2007.

Berntsen, T. K., J. S. Fuglestvedt, M. M. Joshi, K. P. Shine, N. Stuber, M. Ponater, R. Sausen, D. A. Hauglustaine, and L. Li (2005), Response of climate to regional emissions of ozone precursors: Sensitivities and warming potentials, *Tellus, Ser. B*, *57*, 283–304, doi:10.1111/j.1600-0889.2005.00152.x.

Carlton, A. G., R. W. Pinder, P. V. Bhave, and G. A. Pouliot (2010), To what extent can biogenic SOA be controlled, *Environ. Sci. Technol.*, *44*, 3376–3380, doi:10.1021/es903506b.

Collins, W. J., R. G. Derwent, C. E. Johnson, and D. S. Stevenson (2002), The oxidation of organic compounds in the troposphere and their global warming potentials, *Clim. Change*, *52*, 453–479, doi:10.1023/A:1014221225434.

Collins, W. J., S. Sitch, and O. Boucher (2010), How vegetation impacts affect climate metrics for ozone precursors, *J. Geophys. Res.*, *115*, D23308, doi:10.1029/2010JD014187.

Dentener, F., D. Stevenson, J. Cofala, R. Mechler, M. Amann, P. Bergamaschi, F. Raes, and R. Derwent (2005), The impact of air pollutant and methane emission controls on tropospheric ozone and radiative forcing: CTM calculations for the period 1990–2030, *Atmos. Chem. Phys.*, *5*, 1731–1755, doi:10.5194/acp-5-1731-2005.

Derwent, R. G., W. J. Collins, C. E. Johnson, and D. S. Stevenson (2001), Transient behaviour of tropospheric ozone precursors in a global 3-D CTM and their indirect greenhouse effects, *Clim. Change*, *49*, 463–487, doi:10.1023/A:1010648913655.

Derwent, R. G., D. S. Stevenson, R. M. Doherty, W. J. Collins, M. G. Sanderson, and C. E. Johnson (2008), Radiative forcing from surface NO_x emissions: Spatial and seasonal variations, *Clim. Change*, *88*, 385–401, doi:10.1007/s10584-007-9383-8.

Duce, R. A., et al. (2008), Impacts of atmospheric anthropogenic nitrogen on open ocean, *Science*, *320*, 893–897, doi:10.1126/science.1150369.

Felzer, B. S., T. Cronin, J. M. Reilly, J. M. Melilloa, and X. D. Wang (2007), Impacts of ozone on trees and crops, *C. R. Geosci.*, *339*, 784–798, doi:10.1016/j.crte.2007.08.008.

Fiore, A. M., D. J. Jacob, B. D. Field, D. G. Streets, S. D. Fernandes, and C. Jang (2002), Linking ozone pollution and climate change: The case for controlling methane, *Geophys. Res. Lett.*, *29*(19), 1919, doi:10.1029/2002GL015601.

Fiore, A. M., J. J. West, L. W. Horowitz, V. Naik, and M. D. Schwarzkopf (2008), Characterizing the tropospheric ozone response to methane emission controls and the benefits to climate and air quality, *J. Geophys. Res.*, *113*, D08307, doi:10.1029/2007JD009162.

Fiore, A. M., et al. (2009), Multimodel estimates of intercontinental source-receptor relationships for ozone pollution, *J. Geophys. Res.*, *114*, D04301, doi:10.1029/2008JD010816.

Forster, P. M. D., and K. P. Shine (1997), Radiative forcing and temperature trends from stratospheric ozone changes, *J. Geophys. Res.*, *102*, 10,841–10,855, doi:10.1029/96JD03510.

Forster, P., et al. (2007), Changes in atmospheric constituents and in radiative forcing, in *Climate Change 2007: The Physical Science Basis. Contribution of Working Group I to the Fourth Assessment Report of the Intergovernmental Panel on Climate Change*, edited by S. Solomon et al., pp. 129–234, Cambridge Univ. Press, Cambridge, U. K.

Fuglestvedt, J. S., T. K. Berntsen, I. S. A. Isaksen, H. T. Mao, X. Z. Liang, and W. C. Wang (1999), Climatic forcing of nitrogen oxides through changes in tropospheric ozone and methane; global 3D model studies, *Atmos. Environ.*, *33*, 961–977, doi:10.1016/S1352-2310(98)00217-9.

Fuglestvedt, J. S., K. P. Shine, T. Berntsen, J. Cook, D. S. Lee, A. Stenke, R. B. Skeie, G. J. M. Velders, and I. A. Waitz (2010), Transport impacts on atmosphere and climate: Metrics, *Atmos. Environ.*, *44*, 4648–4677, doi:10.1016/j.atmosenv.2009.04.044.

GFDL Global Atmospheric Model Development Team (GFDL GAMDT) (2004), The new GFDL global atmosphere and land model AM2–LM2: Evaluation with prescribed SST simulations, *J. Clim.*, *17*, 4641–4673, doi:10.1175/JCLI-3223.1.

Granier, C., et al. (2011), Evolution of anthropogenic and biomass burning emissions of air pollutants at global and regional scales during the 1980–2010 period, *J. Clim.*, *109*, 163–190, doi:10.1007/s10584-011-0154-1.

Hauglustaine, D. A., and G. P. Brasseur (2001), Evolution of tropospheric ozone under anthropogenic activities and associated radiative forcing of climate, *J. Geophys. Res.*, *106*, 32,337–32,360, doi:10.1029/2001JD900175.

Holland, E. A., and J.-F. Lamarque (1997), Modeling bio-atmospheric coupling of the nitrogen cycle through NO_x emissions and NO_y deposition, *Nutr. Cycl. Agroecosyst.*, *48*, 7–24, doi:10.1023/A:1009710122179.

Horowitz, L. W., et al. (2003), A global simulation of tropospheric ozone and related tracers: Description and evaluation of MOZART, version 2, *J. Geophys. Res.*, *108*(D24), 4784, doi:10.1029/2002JD002853.

Houweling, S., F. Dentener, and J. Lelieveld (1998), The impact of nonmethane hydrocarbon compounds on tropospheric photochemistry, *J. Geophys. Res.*, *103*(D9), 10,673–10,696, doi:10.1029/97JD03582.

Jeuken, A., H. J. Eskes, P. F. J. van Velthoven, H. M. Kelder, and E. V. Holm (1999), Assimilation of total ozone satellite measurements in a three-dimensional tracer transport model, *J. Geophys. Res.*, *104*(D5), 5551–5563, doi:10.1029/1998JD100052.

Jeuken, A., J. P. Veefkind, F. Dentener, S. Metzger, and C. R. Gonzalez (2001), Simulation of the aerosol optical depth over Europe for August 1997 and a comparison with observations, *J. Geophys. Res.*, *106*, 28,295–28,311, doi:10.1029/2001JD900063.

Jonson, J. E., et al. (2010), A multi-model analysis of vertical ozone profiles, *Atmos. Chem. Phys.*, *9*, 26,095–26,142, doi:10.5194/acp-10-5759-2010.

Kunhikrishnan, T., M. G. Lawrence, R. von Kuhlmann, A. Richter, A. Ladstatter-Weissenmayer, and J. P. Burrows (2004), Analysis of tropospheric NO_x over Asia using the model of atmospheric transport and chemistry (MATCH-MPIC) and GOME-satellite observations, *Atmos. Environ.*, *38*, 581–596, doi:10.1016/j.atmosenv.2003.09.074.

Lacis, A. A., D. J. Wuebbles, and J. A. Logan (1990), Radiative forcing of climate by changes in the vertical distribution of ozone, *J. Geophys. Res.*, *95*, 9971–9981, doi:10.1029/JD095iD07p09971.

Leibensperger, E. M., L. J. Mickley, D. J. Jacob, and S. R. H. Barrett (2011), Intercontinental influence of NO_x and CO emissions on particulate matter air quality, *Atmos. Environ.*, *45*, 3318–3324, doi:10.1016/j.atmosenv.2011.02.023.

Levy, H., M. D. Schwarzkopf, L. Horowitz, V. Ramaswamy, and K. L. Findell (2008), Strong sensitivity of late 21st century climate to projected changes in short-lived air pollutants, *J. Geophys. Res.*, *113*, D06102, doi:10.1029/2007JD009176.

Meinshausen, M., et al. (2011), The RCP greenhouse gas concentrations and their extension from 1765 to 2300, *Clim. Change*, *109*, 213–241, doi:10.1007/s10584-011-0156-z.

Ming, Y., V. Ramaswamy, P. A. Ginoux, and L. H. Horowitz (2005), Direct radiative forcing of anthropogenic organic aerosol, *J. Geophys. Res.*, *110*, D20208, doi:10.1029/2004JD005573.

Naik, V., D. Mauzerall, L. Horowitz, M. D. Schwarzkopf, V. Ramaswamy, and M. Oppenheimer (2005), Net radiative forcing due to changes in regional emissions of tropospheric ozone precursors, *J. Geophys. Res.*, *110*, D24306, doi:10.1029/2005JD005908.

Naik, V., D. L. Mauzerall, L. W. Horowitz, M. D. Schwarzkopf, V. Ramaswamy, and M. Oppenheimer (2007), On the sensitivity of radiative forcing from biomass burning aerosols and ozone to emission location, *Geophys. Res. Lett.*, *34*, L03818, doi:10.1029/2006GL028149.

Park, J. H., M. K. W. Ko, C. H. Jackman, R. A. Plumb, J. A. Kaye, and K. H. Sage (Eds.) (1999), M&M-2, NASA: Models and Measurements Intercomparison II, *NASA Tech. Memo*, *NASA TM-1999-209554*, 502 pp.

Pham, M., J. F. Muller, G. P. Brasseur, C. Granier, and G. Megie (1995), A three-dimensional study of the tropospheric sulfur cycle, *J. Geophys. Res.*, *100*(D12), 26,061–26,092, doi:10.1029/95JD02095.

Prather, M. J. (1996), Time scales in atmospheric chemistry: Theory, GWPs for CH_4 and CO, and runaway growth, *Geophys. Res. Lett.*, *23*, 2597–2600, doi:10.1029/96GL02371.

Ramaswamy, V., et al. (2001), Radiative forcing of climate change, in *Climate Change 2001: The Scientific Basis. Contribution of Working Group I to the Third Assessment Report of the Intergovernmental Panel on Climate Change*, edited by J. T. Houghton et al., pp. 349–416, Cambridge Univ. Press, Cambridge, U. K.

Rasch, P. J., M. C. Barth, J. T. Kiehl, S. E. Schwartz, and C. M. Benkovitz (2000), A description of the global sulfur cycle and its controlling processes in the National Center for Atmospheric Research Community Climate Model, Version 3, *J. Geophys. Res.*, *105*(D1), 1367–1385, doi:10.1029/1999JD900777.

Reidmiller, D. R., et al. (2009), The influence of foreign vs. North American emissions on surface ozone in the US, *Atmos. Chem. Phys.*, *9*, 5027–5042, doi:10.5194/acp-9-5027-2009.

Rotman, D. A., et al. (2004), IMPACT, the LLNL 3-D global atmospheric chemical transport model for the combined troposphere and stratosphere: Model description and analysis of ozone and other trace gases, *J. Geophys. Res.*, *109*, D04303, doi:10.1029/2002JD003155.

Rypdal, K., T. Berntsen, J. S. Fuglestvedt, K. Aunan, A. Torvanger, F. Stordal, J. M. Pacyna, and L. P. Nygaard (2005), Tropospheric ozone and aerosols in climate agreements: Scientific and political challenges, *Environ. Sci. Policy*, *8*, 29–43, doi:10.1016/j.envsci.2004.09.003.

Saikawa, E., V. Naik, L. W. Horowitz, J. F. Liu, and D. L. Mauzerall (2009), Present and potential future contributions of sulfate, black and organic carbon aerosols from China to global air quality, premature mortality and radiative forcing, *Atmos. Environ.*, *43*, 2814–2822, doi:10.1016/j.atmosenv.2009.02.017.

Sanderson, M. G., et al. (2008), A multi-model study of the hemispheric transport and deposition of oxidized nitrogen, *Geophys. Res. Lett.*, *35*, L17815, doi:10.1029/2008GL035389.

Schwarzkopf, M. D., and V. Ramaswamy (1999), Radiative effects of CH_4, N_2O, halocarbons and the foreign-broadened H_2O continuum: A GCM experiment, *J. Geophys. Res.*, *104*, 9467–9488, doi:10.1029/1999JD900003.

Seinfeld, J. H., and S. N. Pandis (2006), *Atmospheric Chemistry and Physics - From Air Pollution to Climate Change*, 2nd ed., John Wiley, Hoboken, N. J.

Shindell, D., and G. Faluvegi (2009), Climate response to regional radiative forcing during the twentieth century, *Nat. Geosci.*, *2*, 294–300, doi:10.1038/ngeo473.

Shindell, D. T., G. Faluvegi, N. Bell, and G. A. Schmidt (2005), An emissions-based view of climate forcing by methane and tropospheric ozone, *Geophys. Res. Lett.*, *32*, L04803, doi:10.1029/2004GL021900.

Shindell, D. T., et al. (2008), A multi-model assessment of pollution transport to the Arctic, *Atmos. Chem. Phys.*, *8*, 5353–5372, doi:10.5194/acp-8-5353-2008.

Shindell, D. T., G. Faluvegi, D. M. Koch, G. A. Schmidt, N. Unger, and S. E. Bauer (2009), Improved attribution of climate forcing to emissions, *Science*, *326*, 716–718, doi:10.1126/science.1174760.

Shindell, D. T., M. Schulz, Y. Ming, T. Takemura, G. Faluvegi, and V. Ramaswamy (2010), Spatial scales of climate response to inhomogeneous radiative forcing, *J. Geophys. Res.*, *115*, D19110, doi:10.1029/2010JD014108.

Shine, K. P., J. S. Fuglestvedt, K. Hailemariam, and N. Stuber (2005), Alternatives to the global warming potential for comparing climate impacts of emissions of greenhouse gases, *Clim. Change*, *68*, 281–302, doi:10.1007/s10584-005-1146-9.

Shine, K. P., T. K. Berntsen, J. S. Fuglestvedt, R. B. Skeie, and N. Stuber (2007), Comparing the climate effect of emissions of short- and long-lived climate agents, *Philos. Trans. R. Soc. A*, *365*, 1903–1914, doi:10.1098/rsta.2007.2050.

Sitch, S., P. M. Cox, W. J. Collins, and C. Huntingford (2007), Indirect radiative forcing of climate change through ozone effects on the land-carbon sink, *Nature*, *448*, 791–794, doi:10.1038/nature06059.

Søvde, O. A., C. R. Hoyle, G. Myhre, and I. S. A. Isaksen (2011), The HNO_3 forming branch of the HO_2+NO reaction: Pre-industrial-to-present trends in atmospheric species and radiative forcings, *Atmos. Chem. Phys.*, *11*, 8929–8943, doi:10.5194/acp-11-8929-2011.

Task Force on Hemispheric Transport of Air Pollution (2010), *Hemispheric Transport of Air Pollution*, U. N. Econ. Comm. for Europe, Geneva, Switzerland.

Tie, X. X., S. Madronich, S. Walters, D. P. Edwards, P. Ginoux, N. Mahowald, R. Y. Zhang, C. Lou, and G. Brasseur (2005), Assessment of the global impact of aerosols on tropospheric oxidants, *J. Geophys. Res.*, *110*, D03204, doi:10.1029/2004JD005359.

Unger, N., D. T. Shindell, D. M. Koch, and D. G. Streets (2006), Cross influences of ozone and sulfate precursor emissions changes on air quality and climate, *Proc. Natl. Acad. Sci. U. S. A.*, *103*(12), 4377–4380, doi:10.1073/pnas.0508769103.

Wang, W. C., Y. C. Zhuang, and R. D. Bojkov (1993), Climatic implications of observed changes in ozone vertical distribution in the middle and high latitudes of the Northern Hemisphere, *Geophys. Res. Lett.*, *20*, 1567–1570, doi:10.1029/93GL01318.

West, J. J., A. M. Fiore, V. Naik, L. W. Horowitz, M. D. Schwarzkopf, and D. L. Mauzerall (2007), Ozone air quality and radiative forcing consequences of changes in ozone precursor emissions, *Geophys. Res. Lett.*, *34*, L06806, doi:10.1029/2006GL029173.

West, J. J., V. Naik, L. W. Horowitz, and A. M. Fiore (2009a), Effect of regional precursor emission controls on long-range ozone transport–Part 1: Short-term changes in ozone air quality, *Atmos. Chem. Phys.*, *9*, 6077–6093, doi:10.5194/acp-9-6077-2009.

West, J. J., V. Naik, L. W. Horowitz, and A. M. Fiore (2009b), Effect of regional precursor emission controls on long-range ozone transport–Part 2: Steady-state changes in ozone air quality and impacts on human mortality, *Atmos. Chem. Phys.*, *9*, 6095–6107, doi:10.5194/acp-9-6095-2009.

Wild, O., M. J. Prather, and H. Akimoto (2001), Indirect long-term global radiative cooling from NO_x emissions, *Geophys. Res. Lett.*, *28*(9), 1719–1722, doi:10.1029/2000GL012573.

C. Atherton, Gordon and Betty Moore Foundation, 1661 Page Mill Rd., Palo Alto, CA 94304, USA.

D. Bergmann, Atmospheric Earth and Energy Division, Lawrence Livermore National Laboratory, 7000 East Ave., Livermore, CA 94550, USA.

W. J. Collins, Met Office Hadley Centre, FitzRoy Road, Exeter EX1 3PB, UK.

F. J. Dentener, Institute for Environment and Sustainability, DG-Joint Research Centre, European Commission, TP 280, I-21020 Ispra, Italy.

B. N. Duncan, NASA Goddard Space Flight Center, Greenbelt, MD 20771, USA.

A. M. Fiore, Lamont-Doherty Earth Observatory, 61 Rte. 9W, Palisades, NY, 10964 USA.

M. M. Fry and J. J. West, Department of Environmental Sciences and Engineering, University of North Carolina at Chapel Hill, 146B Rosenau Hall, CB 7431, Chapel Hill, NC 27599, USA. (jasonwest@unc.edu)

P. Hess, Biological and Environmental Engineering, Cornell University, 312 Riley-Robb Hall, Ithaca, NY 14850, USA.

I. A. MacKenzie, School of GeoSciences, University of Edinburgh, King's Buildings, West Mains Road, Edinburgh EH9 3JN, UK.

E. Marmer, Department of Geography, University of Hamburg, Grindelberg 7, 2012, D-20144 Hamburg, Germany.

V. Naik, Atmospheric Physics, Chemistry, and Climate Group, UCAR GFDL, 201 Forrestal Rd., Princeton, NJ 08540, USA.

M. G. Schultz, Institut für Energie- und Klimaforschung (IEK-8), Forschungszentrum Jülich GmbH, D-52425 Jülich, Germany.

M. D. Schwarzkopf, Atmospheric Physics, Chemistry, and Climate Group, NOAA GFDL, 201 Forrestal Rd., Princeton, NJ 08540, USA.

D. T. Shindell, NASA Goddard Institute for Space Studies, 2880 Broadway, New York, NY 10025, USA.

S. Szopa, Laboratoire des Sciences du Climat et de l'Environnement, CEA, IPSL, UVSQ, CNRS, F-91191 Gif-sur-Yvette, France.

O. Wild, Lancaster Environment Centre, Lancaster University, Lancaster LA1 4YQ, UK.

G. Zeng, National Institute of Water and Atmospheric Research, Private Bag 50061, Omakau, Central Otago 9352, New Zealand.